optica

Cycloid scanning for wide field optical coherence tomography endomicroscopy and angiography *in vivo:* supplementary material

KAICHENG LIANG,[1,†] ZHAO WANG,[1,†] OSMAN O. AHSEN,[1] HSIANG-CHIEH LEE,[1] BENJAMIN POTSAID,[1,2] VIJAYSEKHAR JAYARAMAN,[3] ALEX CABLE,[2] HIROSHI MASHIMO,[4,5] XINGDE LI,[6] AND JAMES G. FUJIMOTO[1,*]

[1]*Department of Electrical Engineering and Computer Science, Research Laboratory of Electronics, Massachusetts Institute of Technology, Cambridge MA 02139*

[2]*Thorlabs, Newton, NJ*

[3]*Praevium Research, Santa Barbara, CA*

[4]*Veterans Affairs Boston Healthcare System, Boston, MA*

[5]*Harvard Medical School, Boston, MA*

[6]*Department of Biomedical Engineering, Johns Hopkins University, Baltimore, MD*

[†]*Equal contribution*
**Corresponding author: jgfuji@mit.edu*

Published 11 January 2018

This document provides supplementary information to the article "Cycloid scanning for wide field optical coherence tomography endomicroscopy and angiography *in vivo*" https://doi.org/10.1364/OPTICA.5.000036.

A. Scanner control and software acquisition/display

During imaging, it is important to ensure continuous circular scanning of the piezoelectrically actuated resonant fiber, to avoid transients that would limit volumetric acquisition speeds. Therefore, the sinusoidal outputs were continuously generated from a D/A card (National Instruments (NI) DAQ) to actuate the resonant fiber. The D/A was externally clocked by the swept laser trigger (583490 Hz) to optimize timing synchronizations and accuracy of the generated sinusoidal frequency 7030 Hz. The forward and backward sweep of each laser sweep period were used to generate 2 A-scans. Each circular fiber scan was stored as one frame consisting of a fixed integer number of 166 A-scans.

The micromotor was driven by a vendor-provided board with its own output sampling clock. To optimize synchronization between the micromotor rotation rate and the volumetric acquisition rate, the number of circular frames per volume was one-time empirically tuned such that the volumetric period was approximately equal to the micromotor rotation period. The image acquisition software had a preview mode in which a volume was continuously acquired, processed, and displayed in real time. Tuning of the volumetric period was aided by the software preview, in which the strut fiducial in the *en face* image plane could be observed to be drifting lengthwise if the micromotor and the volumetric rate were not adequately synchronized.

A 'volume trigger' waveform and the two sinusoidal waveforms for driving the piezoelectrically actuated resonant fiber were simultaneously generated from the D/A card using acquisition software (Fig. S1). The volume trigger was a pulse with period equal to the volume period in phase with the sinusoidal waveforms, and triggered the start of a volumetric acquisition. Once the software completed processing and displaying a volume, the A/D card (AlazarTech) read in the next volume trigger for the subsequent acquisition. This ensured that all acquired volumes were synchronized to the same reconstruction parameter ϕ.

The acquisition software used the CPU to process the OCT raw data, therefore the speed was modest and volumetric image preview was limited to ~0.5 volumes/sec. Future work utilizing GPU processing would achieve preview rates limited only by scanner speeds[1]. For data acquisition of single or multiple volumes, the raw data was continuously streamed to memory without processing, such that the volumetric data acquisition rate was the same as the micromotor scanner speed (3 volumes/sec).

B. Image reconstruction

For imaging a large FOV, multiple sequential volumes were continuously acquired starting from a single 'volume trigger' (explained in section A), which resulted in a small accumulated

timing drift due to a small error in either the actual resonant frequency of the fiber scanner or the empirical synchronization of the micromotor rotation speed. This manifested as a 2 A-scan lag per volume (or 2/2322 A-scan lag per frame) for the second and subsequent volumes. The lag could be measured by a 1-D correlation or visual inspection of the first acquired frame of each volume. An alternative way to understand this error is that it results in the subsequent volumes being acquired starting at a slightly later point on the first circular scan of a subsequent volume compared to the first scan of the first volume. This produced a shift in the reconstruction phase ϕ, which is

$$\phi_{drift} = [2 \text{ Ascans}/(166 \text{ Ascans/frame})] \times 2\pi \approx \pi / 36$$

Therefore, for the nth volume reconstruction of a multi-volume sequence, ϕ was offset by $+(n-1)\pi/36$. This error was consistent and could be compensated by a one-time correction. Failure to account for this small error in ϕ resulted in accumulated distortion in subsequent image volumes.

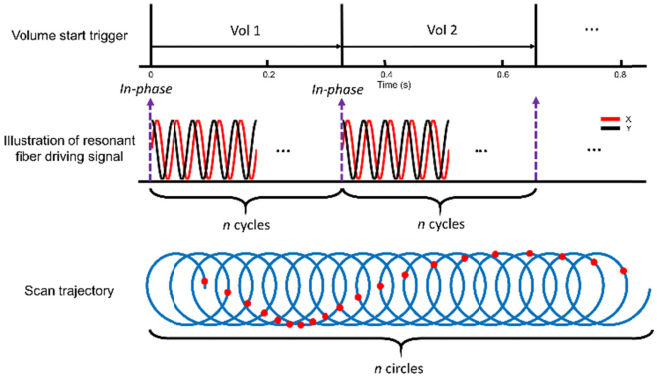

Fig. S1. Timing and driving waveforms of the cycloid scanning protocol. *n* is the number of circular scans per volume and was empirically selected to be 2322 and 13932 to synchronize with the micromotor rotation speed for structural (3 volumes/sec) and angiography imaging (0.5 volumes/sec), respectively.

The entire set of points on the scan trajectory was not required for image reconstruction. The circular scan has the property that it rescans areas already covered by earlier circles in the cycloid trajectory. The leading (left) or trailing (right) half of each circular scan could be used individually for reconstruction. If the entire circular scan was used such that rescanned points were included in the remapping function, distortions would be introduced into the image (Fig. S2(a, d)). This was attributed to the circular scan not being perfectly circular and uniform, resulting in rescanned points producing slightly differing images because the circular scan rotates. The non-telecentricity of the scan also resulted in variation of the optical resolution within the circular scan, producing asymmetry in the scan. In theory, the circularity could be improved by carefully tuning the parameter space of scan amplitudes and phase while monitoring the circularity on a position sensitive detector. However small drifts in the resonant frequency caused by temperature or other fluctuations could potentially lead to non-circularity. Therefore achieving perfect circularity was considered less important than operational simplicity. When processing images using either the trailing (Fig. S2(b, e)) or leading (Fig. S2(c, f)) halves of the circular scan, the scan accuracy observed by scanning a grid appeared acceptable when the two images were assessed separately, but were slightly asymmetric when compared. Combining data from each half, i.e. including data that was rescanned by a later circular scan in the trajectory resulted in distortions. Therefore each volumetric acquisition resulted in two nearly identical volumes, which are separated temporally by the time taken to longitudinally scan through half a circle width, i.e. the time taken for the leading half of the circular scan to rescan the same area that was earlier scanned by the trailing half. For consistency, all data was processed using the leading half-circle. Future work may investigate the potential for dewarping the images to generate a single combined image volume with potentially improved sampling and image quality.

Figure S3 shows a set of 5 sequential volumes acquired as part of a series of 30 volumes, the latter presented in Supplementary Video 1. Figure S3 and Supplementary Video 1 enable an assessment of volume-to-volume repeatability. The 5 volumes as static images do not show apparent differences when assessed by eye, however the Supplementary Video shows small but clearly discernible scan variability. This was due to non-uniform rotational distortion (NURD) of the motor, producing non-constant angular velocity on the slow rotary (circumferential) scan. Increasing the rotary speed can substantially improve NURD while increasing volume rates, and would be especially relevant to smaller diameter devices that have smaller fields of view.

C. OCT angiography processing

The resonantly scanned circular scan frames did not require any rigid or non-rigid registration before computing speckle decorrelation, which is typically required for micromotor-based rotary scanning OCTA. Also, the lag/lead in the fast axis scan speed due to the slow local rotation of the circular scan was very small and thus did not require re-sampling. Rotation of the micromotor at 0.5 Hz was required in order to obtain usable OCTA, which amounted to ~6x Nyquist sampling in the slow scan direction. Significant oversampling was required, to compensate for the undersampling (½ Nyquist) in the fast scan direction and obtain sufficient scan overlap between adjacent frames. The frames were filtered by a 3 x 3 Gaussian kernel before computing decorrelation. Speckle decorrelation was calculated before Cartesian remapping, by element-wise computation using adjacent pairs of raw circular frames with the formula[2]:

$$D_n = 1 - A_n A_{n+1} / \tfrac{1}{2}(A_n^2 + A_{n+1}^2)$$

n is the non-remapped frame number and A_n the OCT amplitude of frame n. A 3-frame moving average of the decorrelation was calculated to reduce noise. The frames were then remapped to a Cartesian grid, similar to the structural data.

D. Cycloid scan efficiency comparison

Efficiency is defined here as being inversely proportional to the time taken for a scan pattern to Nyquist-sample a given area and normalized to the scan area. The efficiency of the cycloid scan is compared to the linear raster scan (ideal efficiency), as well as the

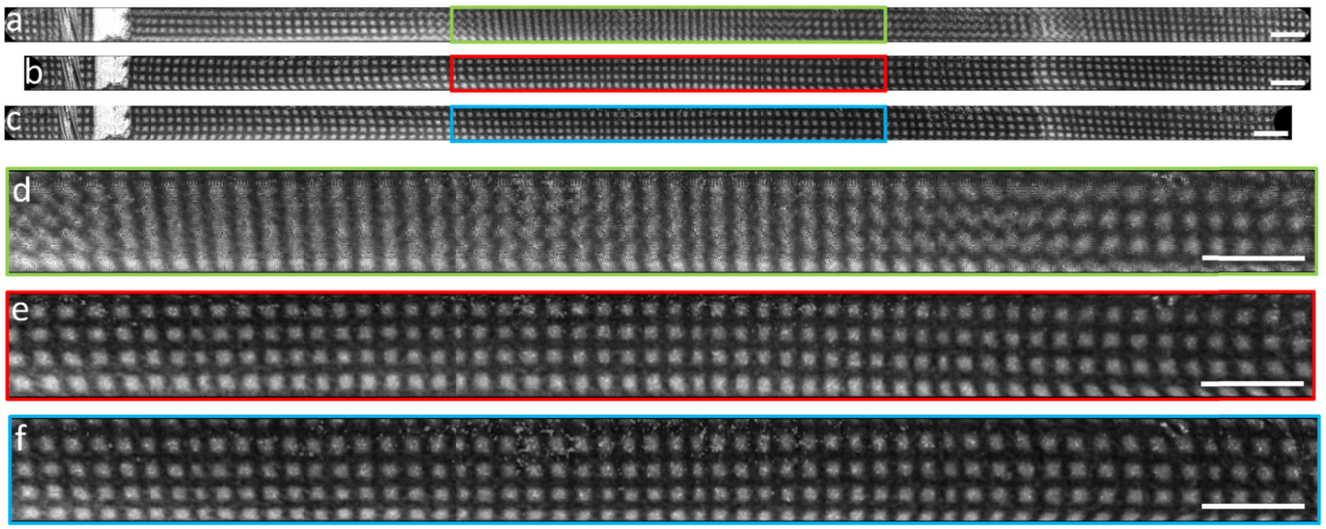

Fig. S2. An image of a printed paper grid with 250 μm pitch, reconstructed using (a) all scanned points, (b) the trailing (right) half of the circular scans, (c) the leading (left) half of the circular scans. (d, e, f) Enlargements showing scan distortions occurring when entire circular scan is used, and slight asymmetry between the use of either half of the scan. Scale bars 1 mm.

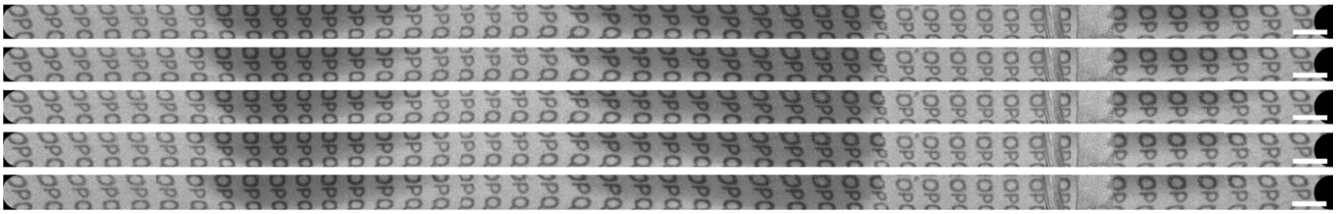

Fig. S3. Sequential volumes of an alphabetically ordered letter grid continuously acquired over the same location, to illustrate repeatability. These volumes are also the first five out of 30 sequential volumes presented in Supplementary Video 1. The small differences between the images may be indiscernible by eye, but are much more clearly appreciated from the video.

sinusoidal raster scan and the spiral scan, which are commonly used resonant scans.

A **linear raster** covering an area of $D \times L$ requires $D/(\omega/2) \times L/(\omega/2)$ A-scans for Nyquist sampling, where D, L, and ω are the width, longitudinal length, and spot size. Therefore the scan time is

$$T_{\text{linear raster}} \propto D/(\omega/2) \times L/(\omega/2) = 4DL/\omega^2 .$$

Normalizing, $\boxed{Efficiency_{\text{linear raster}} \propto \omega^2/4}$.

A **sinusoidal raster** scan has a displacement of $(\mathrm{D}/2)\sin(2\pi t/\tau)$ along the width D, which has period τ and a maximum velocity of $\pi D/\tau$. Let this maximum velocity give Nyquist sampling. Comparing the sinusoidal raster scan to a linear raster scan at this maximum velocity, the former would take $\tau/2$ to cover one width D, while the latter would take τ/π. Therefore the sinusoidal scan is $\pi/2$ slower than the linear raster. The scan time is $T_{\text{sin raster}} \propto 2\pi DL/\omega^2$.

Normalizing, $\boxed{Efficiency_{\text{sin raster}} \propto \omega^2/2\pi}$.

A resonant **spiral scan** requires $\pi D/(\omega/2)$ A-scans in the outermost circle for Nyquist sampling, where D is the diameter. A resonant scanner has a fixed angular velocity producing non-uniform sampling, such that inner circles with smaller circumferences are more densely sampled than outer circles. It also requires $D/2/(\omega/2)$ circles for Nyquist sampling in the radial axis. The scan time is

$$T_{\text{spiral}} \propto \pi D/(\omega/2) \times D/2/(\omega/2) = 2\pi D^2/\omega^2 .$$

Normalizing, $\boxed{Efficiency_{\text{spiral}} \propto \omega^2/8}$. The scan time is the same as the sinusoidal raster (if L = D) but with lower efficiency, and the spiral area is potentially smaller and of order D^2.

A **cycloid scan** requires $\pi D/(\omega/2)$ A-scans in each circle for Nyquist sampling. It also requires $L/(\omega/2)$ circles for Nyquist sampling over the longitudinal strip, when using one half of each circular scan (not using rescanned points). The scan time is

$$T_{\text{cycloid}} \propto \pi D/(\omega/2) \times L/(\omega/2) = 4\pi DL/\omega^2 .$$

An alternate derivation is that the cycloid also has a sinusoidal velocity along the width similar to the sinusoidal scan, but takes τ (twice longer) to cover one width D because the rescan is not used.

Normalizing, $\boxed{Efficiency_{\text{cycloid}} \propto \omega^2/4\pi}$. The cycloid is $\pi/2$ less efficient than the spiral, but has free choice of L for a larger field. The cycloid is twice less efficient than the sinusoidal raster if the rescanned points are not used.

REFERENCES

1. W. Wieser, W. Draxinger, T. Klein, S. Karpf, T. Pfeiffer, and R. Huber, "High definition live 3D-OCT in vivo: design and evaluation of a 4D OCT engine with 1 GVoxel/s," Biomedical Optics Express **5**, 2963-2977 (2014).

2. H.-C. Lee, O. O. Ahsen, K. Liang, Z. Wang, C. Cleveland, L. Booth, B. Potsaid, V. Jayaraman, A. E. Cable, H. Mashimo, R. Langer, G. Traverso, and J. G. Fujimoto, "Circumferential optical coherence tomography angiography imaging of the swine esophagus using a micromotor balloon catheter," Biomedical Optics Express **7**, 2927-2942 (2016).